JACS JOURNAL OF THE AMERICAN CHEMICAL SOCIETY

Article

Magnetic Properties of Cationic Tungsten(IV) Half Sandwich Compounds: Experimental and Theoretical Study of a Solvent and Ligand Stabilized Singlet Ground State Leading to a Thermally Induced Singlet–Triplet Spin State Interconversion

Christian Cremer, and Peter Burger

J. Am. Chem. Soc., **2003**, 125 (25), 7664-7677• DOI: 10.1021/ja028313c • Publication Date (Web): 03 June 2003

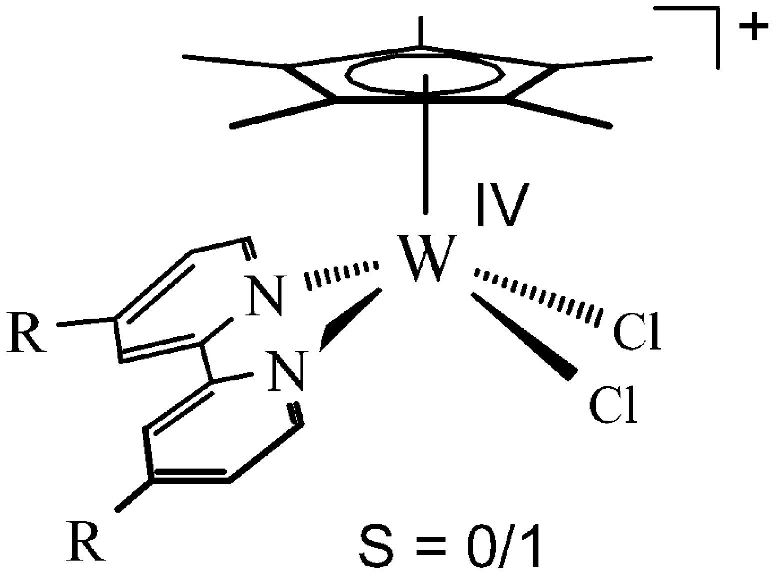

J|A|C|S
ARTICLES
Published on Web 06/03/2003

Magnetic Properties of Cationic Tungsten(IV) Half Sandwich Compounds: Experimental and Theoretical Study of a Solvent and Ligand Stabilized Singlet Ground State Leading to a Thermally Induced Singlet–Triplet Spin State Interconversion

Christian Cremer and Peter Burger*

Contribution from the Anorg.-chem. Institut, Universität Zürich, Winterthurerstr. 190, 8057 Zürich, Switzerland

Received August 28, 2002; Revised Manuscript Received March 10, 2003; E-mail: chburger@aci.unizh.ch

Abstract: A series of novel neutral tungsten(III) and cationic tungsten(IV) complexes with disubstituted 4,4′-R,R-2,2′-bipyridyl (R_2-bpy) ligands of the type $[Cp^*W(R_2\text{-bpy})Cl_2]^{n+}$ (n = 0,1) were prepared and chararacterized by X-ray crystallography. Susceptibility measurements of the tungsten(IV) complexes revealed an intrinsic paramagnetism of these compounds and evidenced different magnetic properties of the dimethylamino and methyl (R = NMe_2, Me) substituted tungsten(IV) compounds in solution and in the solid state. In dichloromethane solution, singlet ground states with thermally populated triplet states were observed, whereas triplet (R = Me) and singlet ground states (R = NMe_2) were observed in the solid state. Using both experimental and theoretical techniques (DFT) allowed to establish solvation and ligand effects to account for the different magnetic behavior. Thermodynamic parameters were derived for the spin equlibria in solution by fits of the temperature dependent ^{1}H NMR shifts to the Van Vleck equation and were found to be in excellent agreement with the DFT calculations.

Introduction

The spin state transition between low and high spin states in organometallic and coordination compounds is in general a well-known process.[1−8] In particular, a large number of detailed studies have been devoted to Fe(II) based systems[1−8] while group 6 transition metal complexes on the other hand have been only rarely investigated.[9,10] Besides earlier NMR-based studies, which have been pursued mostly in the late 1960s and early 1970s,[6−9,11−13] the majority of the magnetic measurements were carried out in the solid state. Therefore, it is not surprising that little attention has been paid to solvation effects on the energetics of the two spin states and was addressed in a quite limited number of experimental studies.[7,8,12−14] Linert et al. for instance recently showed that the high/low spin energy gap in amine donor Fe(II) complexes in solution is strongly influenced by solvation effects.[12,13]

Scheme 1

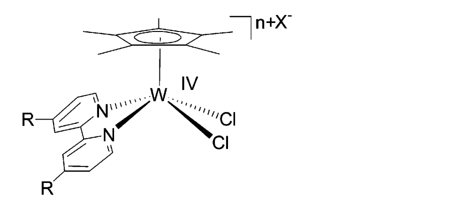

n = 1 X^- = BPh_4^- : R = Me: **1-Me**; R = NMe_2: **1-NMe$_2$**
n = 1 X^- = $B(3,5\text{-}(CF_3)_2\text{-}C_6H_3)_4$: R = H: ^{BArF}**1-H**; R = Me: ^{BArF}**1-Me**
n = 0: R = Me; **2-Me**

Herein, we report on the magnetic properties of half sandwich tungsten(III, IV) compounds, which have been studied both in solution and in the solid state. The position of the singlet–triplet spin equilibrium observed for some of the W(IV) complexes is strongly influenced by solvent and ligand effects and was rationalized through a combination of both experimental and theoretical methods. The presented methodology is conceived as a case study to provide a general guideline for future investigations of this type of systems/phenomena.

Results

The investigated complexes are presented in Scheme 1; their syntheses is described in the next section.

Complex Syntheses. The synthetic access to the cationic pentamethylcyclopentadienyl (Cp*) tungsten(IV) complexes

(1) Goodwin, H. A. *Coord. Chem. Rev.* **1976**, *18*, 293.
(2) Gütlich, P. *Struct. and Bond.* **1981**, *44*, 83.
(3) Gütlich, P.; Hauser, A.; Spiering, H. *Angew. Chem. Int. Ed. Engl.* **1994**, *33*, 2024.
(4) Kahn, O.; Krober, J.; Jay, C. *Adv. Mater.* **1992**, *4*, 718.
(5) König, E. *Struct. Bond.* **1991**, *76*, 51.
(6) Turner, J. W.; Schultz, F. A. *Inorg. Chem.* **2001**, *40*, 5296.
(7) Tweedle, M. F.; Wilson, L. J. *J. Am. Chem. Soc.* **1975**, *98*, 4824.
(8) Dose, E. V.; Murphy, K. M. M.; Wilson, L. J. *Inorg. Chem.* **1976**, *15*, 2622.
(9) Kriley, C. E.; Fanwick, P. E.; Rothwell, I. P. *J. Am. Chem. Soc.* **1994**, *116*, 5224.
(10) Poli, R. *Chem. Rev.* **1996**, *96*, 2135.
(11) Gütlich, P.; McGarvey, B. R.; Kläui, W. *Inorg. Chem.* **1980**, *19*, 3704.
(12) Linert, W.; Enamullah, M.; Gutmann, V.; Jameson, R. F. *Monats. Chem.* **1994**, *125*, 661.
(13) Strauss, B.; Gutmann, V.; Linert, W. *Monats. Chem.* **1993**, *124*, 515.
(14) LaMar, G. *NMR of Paramagnetic Molecules*; Academic Press: New York, 1973.

 10.1021/ja028313c CCC: $25.00

Table 1. Data Collection Parameters of Complexes **1-NMe₂** and **2-Me**

	1-NMe₂	**2-Me**
formula	$C_{48}H_{53}BCl_2N_4W{\cdot}CH_2Cl_2$	$C_{22}H_{27}Cl_2N_2W{\cdot}1/2\ Et_2O$
Fw	1036.43	611.27
habitus	green rect. parallel epiped	violet rect. parallel epiped
crystal dimension [mm]	0.2 × 0.2 × 0.3	0.15 × 0.2 × 0.3
crystal system	monoclinic	triclinic
space group	$P2_1/n$ (no. 14)	P-1 (no. 2)
a [Å]	12.9300(10)	8.369(2)
b [Å]	20.888(2)	10.952(2)
c [Å]	17.632(2)	13.977(3)
α [°]		102.84(3)
β [°]	108.450(10)	101.01(3)
γ [°]		101.60(3)
V [Å^3]	4517.3(8)	1185.7(4)
Z	4	2
ρ_{calc} [g·cm^{-3}]	1.524	1.712
μ [mm^{-1}]	2.83	5.11
F(000)	2096	604
T [K]	183(2)	183(2)
2 $Q\Theta$ [°]	4−52	4−52
no. of measured reflections (total unique)	18000, 5421	20705, 10705
no. of parameters	532	260
$R_1(F^2 > 2\sigma F^2)$	0.0266	0.0318
$wR_2(F^2 > 2\sigma F^2)$	0.0609	0.0776
GOOF, S	1.185	1.042
res. el. dens. [e$^-$Å^{-3}]	1.703, −1.043	1.16, −1.44

$Cp^*W(R_2\text{-bpy})Cl_2^+$, **1-Me** and **1-NMe₂**, where R_2-bpy is a 4,4′-disubstituted 2,2′-bipyridyl donor (R = Me and NMe_2) was previously developed by us from the corresponding trichloride starting materials by chloride abstraction.[15]

Due to difficulties with the purification of the rather insoluble unsubstituted trichloride complex, $Cp^*W(4,4'{-}H_2\text{-bpy})Cl_3$, the latter route proved to be cumbersome for complex **1-H**. We have therefore decided to access **1-H** from the corresponding hitherto unknown tungsten(III) complex, **2-H**, by one-electron oxidation.

Syntheses of 2-H and 2-Me. The novel tungsten(III) complexes **2-H** and **2-Me** were obtained by ligand induced splitting of the dimeric μ-chloro bridged tungsten(III) complex, $(Cp^*WCl_2)_2$ in excellent yields. Because the latter compound was previously described just as a cocrystallized complex with a phosphorus byproduct,[16] we established high yield synthetic access to pure $(Cp^*WCl_2)_2$ by Zn reduction of Cp^*WCl_4 (see experimental). It should be noted that a similar strategy was applied with success by Poli et al. for the synthesis of related mono- and bidentate bisphosphine cyclopentadienyl Mo(III) complexes.[17]

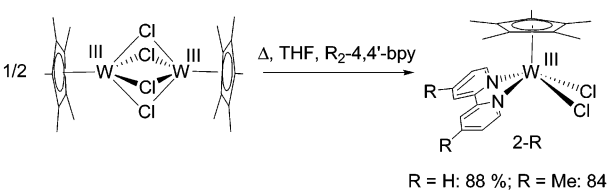

(1)

The dark red tungsten(III) complexes **2-R** were obtained as microcrystalline, analytically pure materials. Their four-legged pianostool geometry was unambiguously confirmed by single-crystal X-ray structure analysis of complex **2-Me** (vide infra).

(15) Cremer, C.; Burger, P. *J. Chem. Soc., Dalton Trans.* **1999**, 1967.
(16) Harlan, C. J.; Jones, R. A.; Koschmieder, S. U.; Nunn, C. M. *Polyhedron* **1990**, *9*, 669.
(17) Abugideiri, F.; Brewer, G. A.; Desai, J. U.; Gordon, J. C.; Poli, R. *Inorg. Chem.* **1994**, *33*, 3745.

Both complexes **2-H** and **2-Me** are paramagnetic and display identical magnetic moments $\mu_{eff} = 1.67\ \mu_B$ at room temperature.

The corresponding cationic tungsten(IV) complex **^{BArF}1-H** was prepared by one-electron oxidation of complex **2-H** with one equiv. of ferrocenium tetraphenylborate followed by metathesis with $NaBAr^F{}_4$ ($BAr^F{}_4 = B(3,5\text{-}(CF_3)_2{-}C_6H_3)_4$) (eq 2).

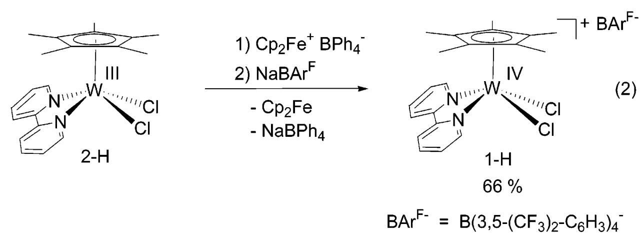

(2)

Complex **^{BArF}1-H** was thus obtained as a microcrystalline, analytically pure dark-green solid.

X-ray Crystal Structure of Complex 1-NMe₂. We have recently reported the X-ray crystal structure analysis of the dimethyl substituted cationic (Cp*) tungsten(IV) complex, **1-Me**.[15] For comparison, an X-ray crystal structure analysis of the corresponding dimethylamino complex, **1-NMe₂**, was sought during the course of this study. The details of the data collection and selected bond distances and angles are summarized in Tables 1 and 2, the molecular structure of **1-NMe₂** is presented in Figure 1.

The coordination geometry of the cationic complex **1-NMe₂** is best described with a square-pyramidal (sq.-py.), i.e., a four-legged pianostool geometry. The closest distance of the tungsten center to the tetraphenylborate counterion is 5.38 Å (W−H), which clearly suggests that complex **1-NMe₂** has a formal 16-electron configuration. As expected, the bipyridyl rings and NMe_2 unit are essentially coplanar; this also explains the inequivalence of the NMe_2 methyl groups observed in the ^{1}H NMR spectrum due to hindered rotation about the N−C$_{aryl}$ bond.

X-ray Crystal Structure of the Tungsten(III) Complex, 2-Me. In addition, we have carried out an X-ray crystal structure

Table 2. Selected Distances [Å] and Angles [deg] of Complexes **1-Me**, **1-NMe$_2$**, and **2-Me**

	1-Me$_2$	1-NMe$_2$	**2-Me$_1$**
W−Cl$_{avg}$	2.361(1)	2.389	2.427
W−N$_{avg}$	2.139(3)	2.12	2.106
W−Z$_{avg}$	2.02	1.97	1.99
N−W−N	73.6(1)	74.7	73.5
Cl−W−Cl	83.1(4)	81.7	82.3
cis-Cl−W−N$_{avg}$	84.5	84.2	83.5
trans-Cl−W−N$_{avg}$	134.2	133.8	132.3
N−W-Z$_{avg}$	113.4	113.3	114.9
Cl−W-Z$_{avg}$	112.2	114.6	112.6

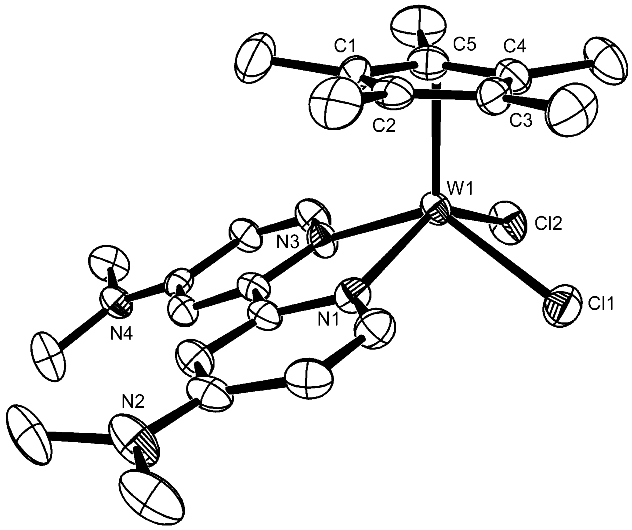

Figure 1. Ortep Plot (50%) level of complex **1-NMe$_2$**. The BPh_4^- counterion has been omitted for clarity.

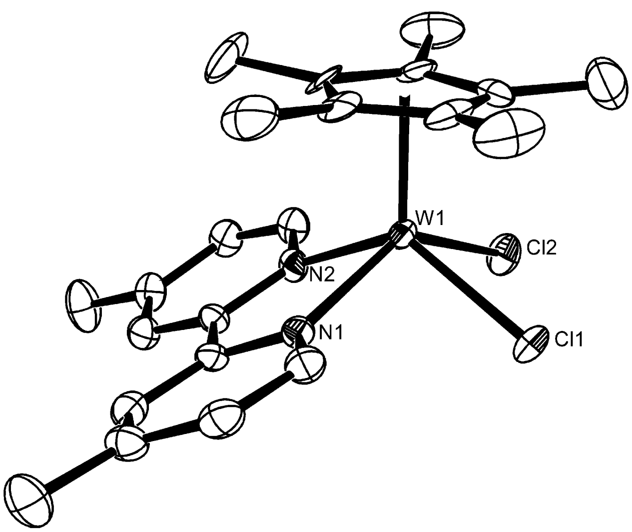

Figure 2. Ortep Plot (50%) level of the neutral tungsten(III) complex **2-Me**.

analysis of the neutral tungsten(III) complex **2-Me**. The molecular structure of **2-Me** is shown in Figure 2, details of the data collection and selected distances and angles are compiled in Tables 1 and 2.

The molecular structure of the neutral tungsten(III) complex **2-Me** strongly resembles its cationic tungsten(IV) congener **1-Me** and also **1-NMe$_2$**. This is best shown by a comparison of the geometrical parameters involving the metal centers of **1-Me**, **2-Me**, and **1-NMe$_2$**, which are compiled in Table 2.

While essentially identical metal centered angles were noticed,

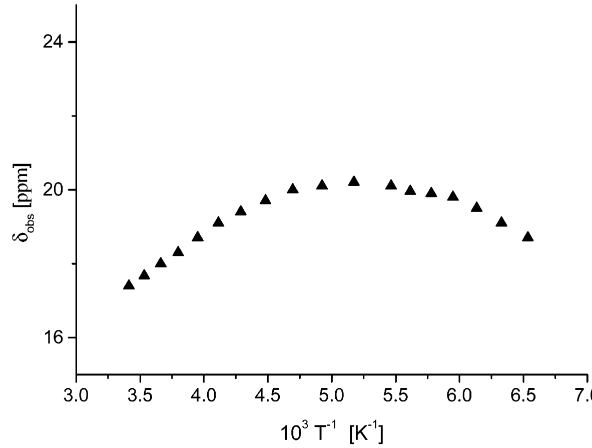

Figure 3. Curie plot of [Cp*W(Me$_2$bipy)Cl$_2$][BPh$_4$] **1-Me** in CD_2Cl_2/CCl_3F (3:1). A similar deviation from linearity is observed for the remaining resonances.

the major difference between the tungsten(III) and tungsten(IV) complexes are the tungsten chloride bond distances, which are 0.06 Å shorter in the cationic complex **1-Me** than in the corresponding neutral compound **2-Me** suggesting stronger π-donation of the chloride ligands to the more Lewis-acidic cationic tungsten center. As will be elaborated later on in the discussion section, the large deviation of the W−C$_{Cp*}$ distances observed in the complexes described herein is a major feature of these compounds.

Temperature, Solvent and Anion Dependent ^{1}H NMR Studies of Complexes 1-R and 2-Me. (a) Temperature Dependence in CD_2Cl_2 Solution. The dispersion of the ^{1}H NMR chemical resonances in complexes **1-R** clearly evidenced the intrinsic paramagnetism of these compounds. This is best exemplified with the chemical shift range of ±100 ppm observed for the ^{1}H NMR resonances of **1-Me** in CD_2Cl_2 at RT. This prompted us to investigate the temperature dependence of the ^{1}H NMR chemical shifts. In exemplary fashion this is shown for the vt ^{1}H NMR chemical shift of the Cp* methyl resonance in **1-Me** plotted vs reciprocal temperature (Figure 3), which was recorded in a CD_2Cl_2/CCl_3F mixture to reach lower temperatures. A comparison with data obtained in pure CD_2Cl_2 showed no significant influence of the solvent mixture on the ^{1}H NMR chemical shifts.

The strong deviation of the chemical shifts vs T^{-1} from linearity, which was also observed for the remaining ^{1}H NMR resonances (not shown), immediately demonstrated the *non-Curie* behavior of complex **1-Me** (Figure 3). Similar results were obtained for the dimethylamino substituted complex **1-NMe$_2$** although the dispersions of its ^{1}H NMR chemical shifts were appreciably smaller. The magnetic behavior of the substituted bipyridyl complexes **1-Me** and **1-NMe$_2$** in CD_2Cl_2 solution was therefore clearly distinguishable from a *pure* triplet state. Prior to our DFT calculations of these systems, which also prompted us to investigate the unsubstituted bipyridyl complex **1-H**, we intended to establish that a Curie behavior could be observed in these square pyramidal tungsten halfsandwich complexes after all. Therefore, we studied the temperature dependence of the ^{1}H NMR shifts of the corresponding neutral tungsten(III) complex **2-Me** in solution which is shown for one of the five resonances in Figure 4.

As anticipated, the ^{1}H NMR shifts of the open shell $S = 1/2$ tungsten(III) complex **2-Me** displayed an excellent linear

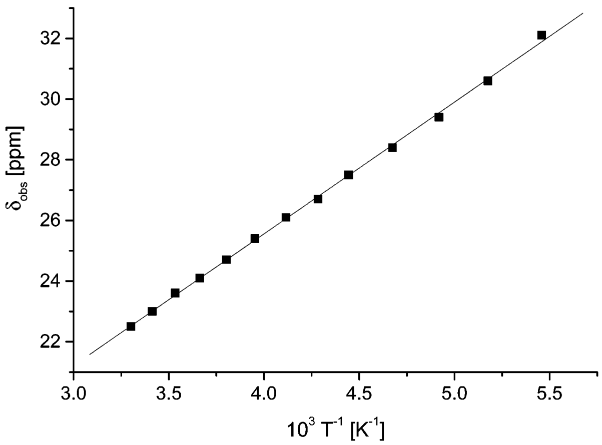

Figure 4. 1/*T* dependence of the ^{1}H NMR resonances of tungsten(III) complex **2-Me** in CD_2Cl_2. (R^2 = 0.999).

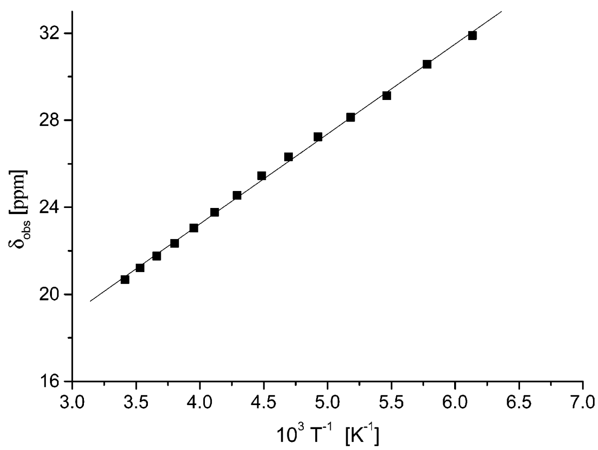

Figure 5. Curie behavior of **1-H** (shown for the Cp* methyl proton shift) in CD_2Cl_2. Linear regression (- -) with R^2 = 0.999.

dependence on the reciprocal temperature (Figure 4). This clearly substantiated that an agreement with the Curie-law could be in principle also observed in complexes **1-Me** and **1-NMe$_2$**, provided that the cationic tungsten(IV) systems had a *pure* triplet state.

Prior to the measurements of the unsubstituted complex **1-H**, this rationale was confirmed by the results of our DFT calculations. The latter also suggested the possibility to induce a change of the position of the spin-state equilibrium through different substitutents R of the 4,4′−R_2-bpy ligands (vide infra). We have therefore also recorded vt ^{1}H NMR spectra of the unsubstituted bipyridyl tungsten(IV) complex **1-H** (Figure 5).

The inspection of the temperature dependent ^{1}H NMR chemical shifts vs T^{-1} data of **1-H** clearly revealed the *Curie behavior* of this complex (Figure 5), which was fully consistent with the trend predicted by our theoretical calculations.

(b) Anion Dependence. The temperature dependence of the ^{1}H NMR chemical shifts of the analogue of **1-Me**, complex **^{BArF}1-Me** with the more weakly coordinating anion was also investigated in CD_2Cl_2 solvent (Figure 6).

Despite some minor difference in the curvatures and changes of the chemical shifts, the δ vs T^{-1} plots for the cationic 4,4′-Me_2-bipyridyl complexes **1-Me** and **^{BArF}1-Me** presented in Figure 6 are essentially identical. A strong deviation from the Curie behavior (linearity) is therefore also attributable to complex **^{BArF}1-Me**. Hence, this measurement clearly revealed

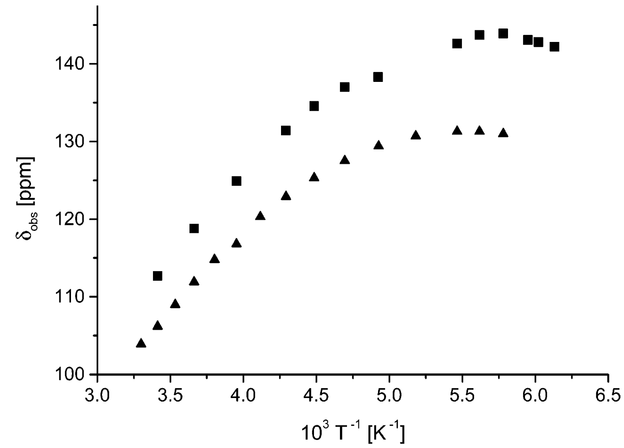

Figure 6. 1/*T*-dependence of the *Me$_2$*bipy chemical shifts Protonen in [Cp*W(Me_2bipy)Cl_2][X] **1-Me** (X = BPh_4^-) and **^{BArF}1-Me** (X = BAr^F) (■) in CD_2Cl_2.

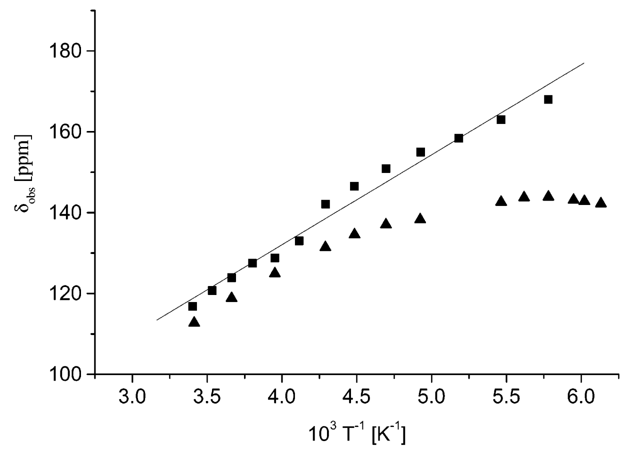

Figure 7. 1/*T* dependence of the ^{1}H NMR chemical shifts of the *Me$_2$*bipy protons in [Cp*W(Me_2bipy)Cl_2][BAr^F] **^{BArF}1-Me** in CD_2Cl_2 (▲) and in a toluene-d_8/CD_2Cl_2 (2:1) mixture (■) (R^2 = 0.978).

that the temperature dependent ^{1}H NMR chemical shifts are essentially *independent* of the *counterion*.

(c) Mixtures of CD_2Cl_2/Toluene (1:2 v/v). To probe for the polarity dependence of the spin-state transition equilibrium in complex **1-Me**, we recorded vt ^{1}H NMR spectra of complex **^{BArF}1-Me** in a CD_2Cl_2/toluene 1:2 (v/v) mixture. Due to the rather low solubility of the cationic complexes, the usage of the partially fluorinated BAr^F anion was a prerequisite for these measurements. The plot of the chemical shift for the bipyridyl methyl group vs reciprocal temperature is shown in Figure 7.

Although the plot presented in Figure 7 displayed a slight curvature, a linear T^{-1} dependence of the chemical shifts can be conceived with good confidence (R^2 = 0.978). Therefore, in sharp contrast to the results observed in pure CD_2Cl_2 solvent (data are included for comparison in Figure 7), a *Curie behavior* can be attributed to complex **^{BArF}1-Me** in this significantly *less polar solvent* mixture.

(d) Concentration Dependence including UV/Vis Spectral and Molar Conductivity Data. The ^{1}H NMR chemical shifts of complex **1-Me** in CD_2Cl_2 displayed a negligible concentration dependence (± 2 ppm), which was evidenced through measurements at 10^{-1} and 10^{-3} M concentrations. Further support for the absence of a chemical equilibrium was established through the perfect Lambert−Beer behavior of the absorptions of the deeply green colored complex **1-Me** in the UV/Vis spectra measured in the concentration range of $10^{-5}-10^{-3}$ M. In addition, concentration dependent molar conductivity measurements (not shown) were performed for **1-Me**[15] The molar conductivity of $\Lambda_m = 58$ S·cm^2·mol^{-1} at 10^{-4} molar concentration,[15] together with the observed [**1-Me**]$^{1/2}$ concentration dependence (range of $10^{-3}-10^{-5}$ M) in dichloromethane clearly allowed to establish that **1-Me** behaves as an 1:1 electrolyte. It can be therefore described with a formal 16-electron configured tungsten center.

Determination of Thermodynamic Parameters. At the outset of this section, it should be emphasized that the observed temperature induced ^{1}H NMR spectral changes for all compounds described herein are fully reversible. The determination of the thermodynamic parameters for the singlet triplet equilibrium, $S \rightarrow T$, in complexes **1-Me** and **1-NMe$_2$** was initially attempted by a fit of the temperature dependence of the observed ^{1}H NMR chemical shifts, δ_{obs} (H_{obs}) to eq 3 using the Van-Vleck equation in the form applied by Rothwell et al. for their successful fit of a tungsten(IV) singlet−triplet spin-equilibrium in toluene solution.[9]

$$H_{obs} = H_{dia} + \frac{H_O \cdot A \cdot g \cdot \beta \cdot (6 \cdot e^{-E/kT})}{(\gamma_H/2\pi) \cdot 3 \cdot k \cdot T \cdot (1 + 3 \cdot e^{-E/kT})} \qquad (3)$$

However, severe problems with the fits to this equation for complex **1-Me** (details see discussion section) let us resort to the more general eq 4. The relation between eqs 3 and 4 arises from the proper treatment of entropy terms. In addition, the free enthalpy change of solvation is not properly accounted for in eq 3. Equation 4 was originally derived by Eaton et al.[18] and revised later by Horrocks et al.[19] It has to be stressed that this treatment is only appropriate if the observed paramagnetic shifts can be solely attributed to a *contact-shift*, i.e., *through bond* term.[14] The justification of this assumption for complexes **1-Me** and **1-NMe$_2$** will be provided in the discussion section

$$\delta_{obs} = \delta_{dia} + \frac{A \cdot \gamma_e \cdot g \cdot \beta}{\gamma_H \cdot 3 \cdot k \cdot T \cdot (1 + e^{(\Delta H - T\Delta S)/RT})} \qquad (4)$$

Here γ_e, γ_H are the gyromagnetic ratios of the electron and proton. β is the Bohr magneton, k is the Boltzmann constant, g is the g-factor of the unpaired electron, A is the hyperfine splitting constant of the observed proton, ΔH is the enthalpy, and ΔS is the entropy change for the singlet triplet spin equilibrium.

The quality of the fit can be estimated from the optimized values for the proton resonances, which should lead to different values for $\delta_{dia,i}$ and A_i for the individual proton sites i, but to the same values for ΔH and ΔS. Additionally, the fit can be checked by inspection of the derived optimized chemical shifts $\delta_{dia,i}$. For a reasonable fit, the values of $\delta_{dia,i}$ are expected to be in the range of the corresponding diamagnetic compounds/free ligands and should display small esd's. The fits of the temperature dependent ^{1}H NMR shifts for complexes **1-Me** and **1-NMe$_2$** are presented in Figures 8 and 9; the derived values for the optimized parameters are summarized in Tables 3 and 4.

(18) Eaton, D. R.; Phillips, W. D.; Cadwell, D. J. *J. Am. Chem. Soc.* **1963**, *85*, 397.
(19) Pignolet, L. W.; Horrocks, W. D., Jr. *J. Am. Chem. Soc.* **1969**, *91*, 3976.

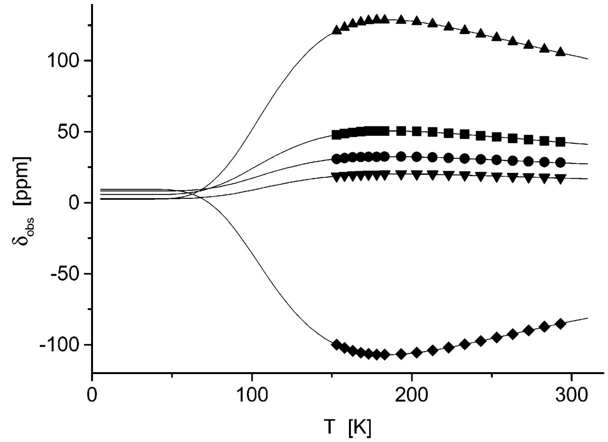

Figure 8. Temperature dependence of the ^{1}H NMR chemical shifts δ_{obs} in [Cp*W(Me$_2$bipy)Cl$_2$][BPh$_4$] **1-Me**: -Me$_{bipy}$ (▲), H$_{arom}$ (■, ●, ◆) und Cp* (▼). The fitting curves were derived using eq 4.

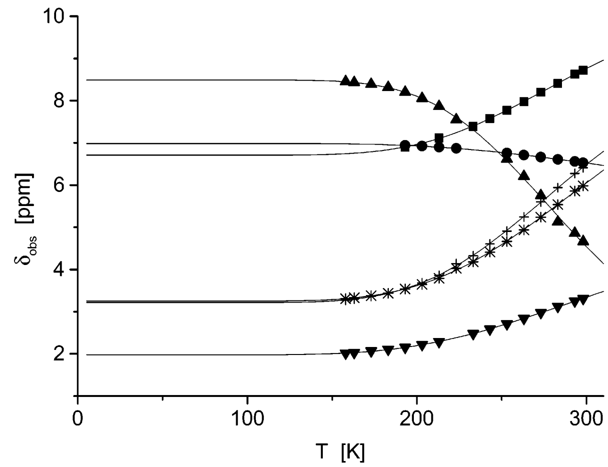

Figure 9. Temperature dependence of the proton chemical shifts in [Cp*W-((NMe$_2$)$_2$bipy)Cl$_2$][BPh$_4$] **1-NMe$_2$**: H$_{arom}$ (■, ●, ▲), −NMe$_2$ (+, ∗) und Cp* (▼). The fitting are based on eq 4.

Table 3. Diamagnetic Chemical Shifts δ_{dia} Hyperfine Coupling Constants A with esd's for the Protons in [Cp*W(R$_2$Bipy)Cl$_2$][BPh$_4$] **1-Me** and **1-NMe$_2$**

1-Me	$_d\delta_{ia}$ [ppm]	A [MHz]	1-NMe$_2$	δ_{dia} [ppm]	A [MHz]
H$_{arom}$	9 ± 3	+ 0.56 ± 0.03	H$_{arom}$	8.49 ± 0.04	+ 0.05 ± 0.01
H$_{arom}$	8 ± 2	− 0.12 ± 0.01	H$_{arom}$	6.99 ± 0.01	+ 0.01 ± 0.01
H$_{arom}$	6 ± 3	− 0.28 ± 0.03	H$_{arom}$	6.71 ± 0.02	− 0.04 ± 0.01
-Me$_{bipy}$	2 ± 4	− 0.56 ± 0.03	-NMe$_2$	3.25 ± 0.01	− 0.07 ± 0.01
Cp*	3 ± 1	− 0.09 ± 0.01	-NMe$_2$	3.22 ± 0.02	− 0.06 ± 0.01
			Cp*	1.98 ± 0.01	− 0.04 ± 0.01

Table 4. Averaged Thermodynamic Parameters with esd's for the Singlet−Triplett Spin State Equilibrium and Estimated Based Thereon and Experimental Effective Magnetic Moments of [Cp*W(R$_2$Bipy)Cl$_2$][BPh$_4$] **1-Me**, **1-NMe$_2$**

complex	ΔH [kJ mol^{-1}]	ΔS [Jmol^{-1}K^{-1}]	$\mu_{eff,\ calc.}$ [μ_B]	$\mu_{eff,\ exp}$ [μ_B]
4-Me	4.5 ± 0.1	29 ± 1	2.10	2.02^b
4-NMe$_2$	14 ± 1	37 ± 7	0.58	0.64^a

Using the derived thermodynamic parameters, spin equilibrium constants ($S \rightarrow T$) of $K = 10^6$ for **1-Me** and $5 \cdot 10^{-5}$ for complex **1-NMe$_2$** can be derived at RT. Using these values and $\mu_{eff,triplet} = 2.49$ μ_B from the solid-state measurements for the pure triplet and $\mu_{singlet} = 0$ for the singlet states, this allowed to estimate the effective magnetic moments $\mu_{eff,calc}$ in CD_2Cl_2

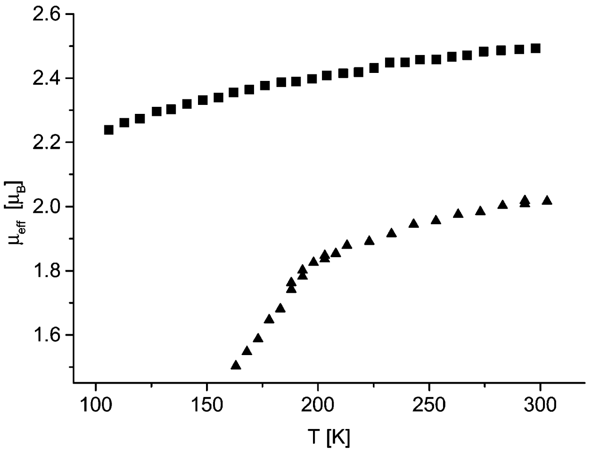

Figure 10. Temperature dependence of the effective magnetic moment μ_{eff} of [Cp*W(Me$_2$bipy)Cl$_2$][BPh$_4$] **1-Me** in the solid state (■) and in solution (▲, Evans method).

solution. A comparison of the experimentally determined values in solution (Evans method) and the estimated magnetic moments ($\mu_{eff,exp}$ and $\mu_{eff,calc}$) established the excellent agreement of these data (Table 4). This clearly validated the experimentally determined thermodynamic parameters.

VT magnetic susceptibility measurements of 1-Me and 1-NMe$_2$ in the solid state and solution (Evans method): Solid-state magnetic susceptibility measurements for complexes **1-Me** and **1-NMe$_2$** were performed in the temperature range from 4 to 300 K. The temperature-dependent effective magnetic moment of complex **1-Me** presented in Figure 10 clearly evidenced a *triplet* ground state with zero-field splitting and an effective magnetic moment, $\mu_{eff} = 2.49\ \mu_B$ in the solid state at room temperature.

The vt magnetic moment data of complex **1-Me** in *dichloromethane* were derived from magnetic susceptibility data in solution by the Evans method,[20,21] (see exp. for details) and are also included in Figure 10. An inspection of Figure 10 immediately revealed that the CH_2Cl_2 solution data are in sharp contrast to the solid-state measurements. In solution, a strong deviation from linearity and significant smaller values of the effective magnetic moment μ_{eff} vs temperature data were observed. Note, that this is consistent with the aforementioned temperature dependence of the ^{1}H NMR chemical shifts of **1-Me** in CD_2Cl_2 solution.

Finally, vt solid-state magnetic susceptibility data for complex **1-NMe$_2$** showed that the dimethylamino substituted complex is *diamagnetic* in the temperature range from 10 to 300 K. This result slightly deviated from our magnetic susceptibility data measured at 298 K with a Johnson-Matthey laboratory magnetic balance, which gave a reproducible value of $\mu_{eff} = 0.52\ \mu_B$. Although we have no explanation for this slight difference, both results clearly provided evidence for the reduced magnetic moment of complex **1-NMe$_2$** compared to its methyl substituted congener **1-Me**.

DFT Calculations and MO Analyses of Complexes 1-R. The coordinates of the cationic metal complexes **1-Me** and **1-NMe$_2$** observed in the X-ray crystal structures, with the C−H bonds set to 1.1 Å, were used as starting geometries. These structures were optimized using the open shell unrestricted formalisms at the density functional theory (DFT) level and the nonlocal Becke-Perdew-86 functional.[22,23] The RI-J method implemented in the RIDFT[24,25] program of Turbomole[26] program suite was applied with the spin occupations fixed at either the singlet ($S = 0$) or triplet ($S = 1$) spin state. The amount of spin contamination was carefully monitored by the inspection of the expectation value of the spin operator $\langle S^2\rangle\cdot\langle S^2\rangle$ was found in all cases to be 2.00 ± 0.01 for the triplet states and 0.00 ± 0.01 for the singlet states, thus evidencing negligible contributions of higher spin states. A Stuttgart-Dresden (ecp-60-mwb) pseudopotential[27] was used throughout in these calculations for the tungsten center and the structures were initially optimized using a TZVP[28] basis set for W and SVP[29] basis sets for the residual atoms. After convergence, optimization was continued with the large TZVP basis applied to all atoms; usually this required just a few steps to converge. For the methyl substituted complex **1-Me** the singlet and triplet state optimized geometries (TZVP basis) were characterized as true minima through the calculation of the numerical second derivatives (finite differences), which displayed the absence of imaginary vibrations. In addition, we performed geometry optimizations with the unrestricted hybrid UB3LYP functional[30] using a TZVP basis for all atoms and the structures optimized with the BP86 functional as starting geometries. Final relative energies of these calculations are summarized in Table 5.

Table 5. DFT Derived Total and Relative Energies (in parentheses) of Complexes **1-R** in [Hartree] and [kJ/mol]

	$S = 0$	$S = 1$
1-Me^{a})	−1952.160651	−1952.167339 (−17.6)
1-Me^{rotaa})	−1952.159857 (+2)	
1-Me^{tbpy}(II)^{a}	−1952.1352275 (+67)	
1-Me^{iso}(III)^{a}	−1952.1252866 (+92)	
1-Me^{b}	−1951.1220302	1951.1315935 (−25.0)
1-H^{a}	−1873.49162912	1873.497976 (−16.7)
1-NMe$_2$^{a}	−2141.561919	−2141.56705 (−12.5)
1-NMe$_2$^{b}	−2140.3946289	−2140.4016170 (−16.7)

^{a} BP86 functional. ^{b} B3LYP functional.

Further evidence for the higher stability of the triplet states of complexes **1-H**, **1-Me**, and **1-NMe$_2$** in the *gasphase* was provided through SCF-instability calculations of the $S = 0$ states, which were performed with the ESCF module[31] of the Turbomole program package. This was manifested through the observation of *triplet instabilities* for the converged wave functions of the singlet states of these complexes.

Furthermore, we performed calculations for the hypothetical pseudo-trigonal biypyramidal (tbpy) isomer, **1-Me^{tbpy}** presented in Figure 11. The geometry was constrained to C_s symmetry containing the chlorine and tungsten atoms in the symmetry plane, since the geometry optimization collapsed otherwise to the pianostool geometry, i.e., **1-Me**. In addition, we performed

(20) Evans, D. F. *J. Chem. Soc.* **1959**, 2003.
(21) Schubert, E. M. *J. Chem. Educ.* **1992**, *69*, 62.
(22) Becke, A. D. *Phys. Rev. A* **1988**, *38*, 3098.
(23) Perdew, J. P. *Phys. Rev. B* **1986**, *33*, 8822.
(24) Eichkorn, K.; Treutler, O.; Öhm, H.; Häser, M.; Ahlrichs, R. *Chem. Phys. Lett.* **1995**, *242*, 652.
(25) Eichkorn, K.; Treutler, O.; Öhm, H.; Häser, M.; Ahlrichs, R. *Chem. Phys. Lett.* **1995**, *240*, 283.
(26) Ahlrichs, R.; Bär, M.; Häser, M.; Horn, H.; Kölmel, C. *Chem. Phys. Lett.* **1989**, *162*, 165.
(27) Andrae, D.; Häussermann, U.; Dolg, M.; Stoll, H.; Preuss, H. *Theor. Chim. Acta* **1990**, *77*, 123.
(28) Schäfer, A.; Huber, C.; Ahlrichs, R. *J. Chem. Phys.* **1994**, *100*, 5829.
(29) Schäfer, H.; Ahlrichs, R. *J. Chem. Phys.* **1992**, *97*, 1992.
(30) Becke, A. D. *J. Chem. Phys.* **1993**, *98*, 5648.
(31) Weiss, H.; Ahlrichs, R.; Häser, M. *J. Chem. Phys.* **1993**, *99*, 1262.

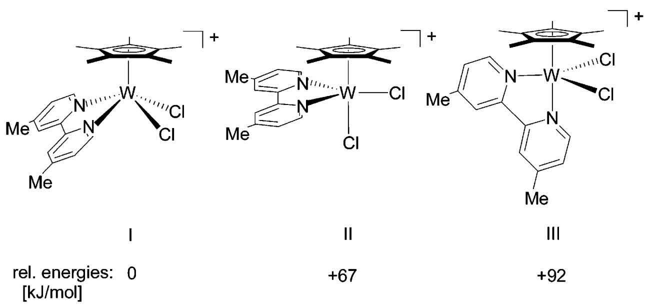

Figure 11. DFT derived relative energies of geometry optimized isomers of $[Cp^*W(Me_2bipy)Cl_2]^+$ **1-Me** ($S = 0$) (DFT).

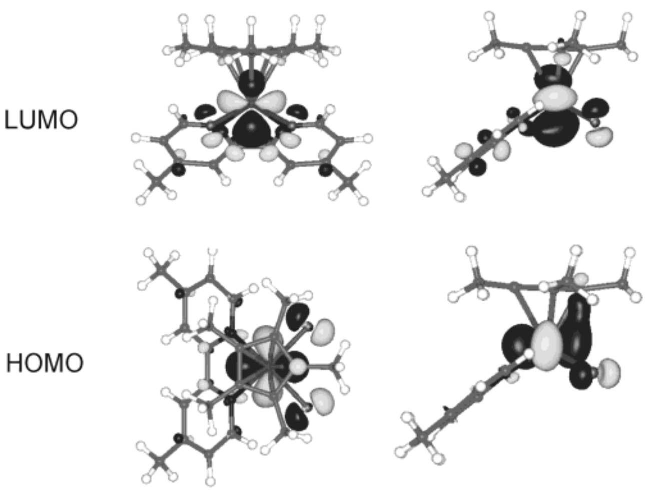

Figure 12. 12. HOMO and LUMO for the $S = 0$ state of **1-Me**.

a geometry optimization of another pseudo-trigonal biypyramidal isomer, i.e., **1-Me**[**iso**] using again C_s symmetrical constraints with the N and W atoms spanning the symmetry plane. The relative energy of the geometry optimized structure of **1-Me**[**iso**] is also included in Figure 11.

In addition, we inspected the frontier orbitals of complex **1-Me**. The molecular orbitals of the HOMO and LUMO of the singlet state ($S = 0$) are presented in Figure 12.

We also analyzed the equivalent molecular orbitals (MOs) of the corresponding triplet state of **1-Me**, i.e., the second highest, single occupied molecular orbital, SSHOMO, and the SHOMO. As anticipated, the same ordering and shape of the orbitals was observed; therefore the MOs shown in Figure 12 for the singlet state of **1-Me** are also a applicable to the corresponding orbitals of the $S = 1$ state.

Furthermore, we analyzed the HOMO−LUMO gaps ($\Delta_{S=0}$), of the singlet states and the energy differences $\Delta_{S=1}$ between the SSHOMO and the SHOMO levels in the $S = 1$ states ($\Delta_{S=1} = E_{\mathrm{SHOMO}} - E_{\mathrm{SSHOMO}}$). The values of $\Delta_{S=0}$ in complexes **1-R** are appreciably small and in the narrow range of 0.28−0.30 eV. For the energy differences, $\Delta_{S=1}$ the order **1-H** (0.47) < **1-Me** (0.48) < **1-NMe$_2$** (0.64) with the energies given in parentheses in [eV] is observed.

DFT Calculations—solvent Effects. The effect of solvation on the energy differences between the triplet and singlet state were probed using a dielectric continuum approach. Because the COSMO solvation method developed by Klamt[32] et al. was not implemented for unrestricted open-shell calculations in version 5.3 of Turbomole, the density functional program package DMOL was sought as an alternative. Unfortunately, usage of relativistic ECP's is not available for COSMO calculations in the current version of DMOL.[33] We therefore performed all-electron calculations, in which scalar relativistic effects for all atoms were included using the approach described by Delley et al. (VPSR keyword).[34] The methylenechloride solvent was modeled with a dielectric constant of $\epsilon = 8.9$ (at $T = 298$ K) and using a probe radius of 2.3 Å.[35] Both the singlet and triplet states of **1-Me** were fully optimized applying dnp basis sets for all atoms using the COSMO implementation and a BP86 functional with the standard convergence criteria of DMOL. Final total energies are tabulated in Table 6.

In addition, we performed calculations with the Jaguar rel. 4.1 program package[36] using the self-consistent reaction field (SCRF) approach implemented in Jaguar.[37] A LACV3P basis set including a Hay-Wadt scalar relativistic pseudopotential for the tungsten metal center and 6-31G** basis sets for the residual atoms and the BP86 functional were used. The aforementioned BP86 and UBP86 optimized gasphase structure (TZVP basis) of complex **1-Me** were used as starting geometries and required just a few geometry optimization cycles to converge with the BP86 ($S = 0$) and UBP86 ($S = 1$) functionals. In a next step, the geometries were also optimized including solvation by dichloromethane at 298 K. The temperature dependent change of the solvent was modeled at 180 K using experimental density and permittivity data of dichloromethane at this temperature from the literature.[38] The derived relative energies for both spin states are also summarized in Table 6.

Table 6. Relative Energies in kJ/mol of the Singlet and Triplet Spin States of Complex **1-Me** in the Gas Phase and in Dichloromethane Solution

	$S = 1$	$S = 0$
gas phase[a]	0	+15
CH_2Cl_2 solution[a] $T = 298$ K, $\epsilon = 8.9$, $d = 1.325$ [a]	0	+6.7
CH_2Cl_2 solution[a] $T = 180$ K, $\epsilon = 16.3$, $d = 1.573$[a]	0	+1
dichloromethane solution (RT, $\epsilon = 8.9$)[b]	0	−12

[a] Jaguar 4.1 calculations (see text). [b] DMOL calculations (see text).

Discussion

In a recent account Poli reviewed the chemistry of open-shell paramagnetic organometallic complexes.[10] This clearly evidenced that little attention has been paid to the magnetic properties, in particular spin state transitions, of tungsten d^2 metal complexes, i.e., in their tetravalent oxidation state, while molybdenum(IV) complexes were studied in some detail by the author.[10,17] In principle, one might infer that halfsandwich complexes with a d^2-electron configuration could be intrinsically *diamagnetic*. In fact, however, quite frequently just the opposite is observed, and in the aforementioned review R. Poli discusses

(32) Klamt, A. *J. Phys. Chem.* **1995**, *99*, 2224.

(33) Andzelm, J.; Kölmel, C.; A., K. *J. Chem. Phys.* **1995**, *103*, 9312.
(34) Delley, B. *Int. J. Quantum Chem.* **1998**, *69*, 423.
(35) This value was estimated using the formalism prescribed in Jaguar, i.e., from $r^3 = 3/4\pi \cdot (M/N_a) \cdot \Delta/\rho$, where M is the molecular weight of dichloromethane (85.9 g/mol), N_a is Avogadro's number, Δ is the packing density, which was set to 0.5, and ρ is the density of the dichloromethane.
(36) Jaguar 4.1, Schrödinger., Inc., Portland, OR, 1991−2001.
(37) Tannor, D. J.; Marten, B.; Murphy, R.; Friesner, R. A.; Sitkoff, D.; Nicholls, A.; Rignalda, M.; Goddard, W. A., III; Honig, B. *J. Am. Chem. Soc.* **1994**, *116*, 11 875.
(38) Morgan, S. O.; Lowry, H. H. *J. Phys. Chem.* **1930**, *34*, 2385.

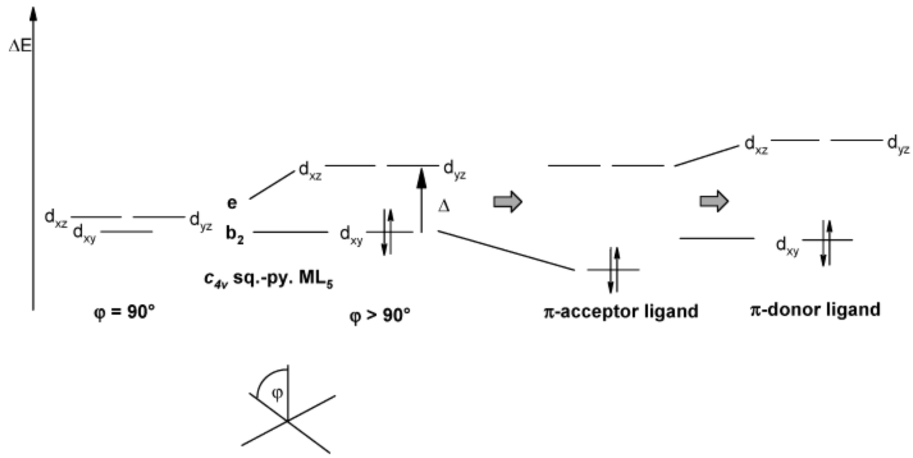

Figure 13. Molecular orbital scheme in sq.-pyramidal geometry.

aspects when to expect open shell systems.[10] At the risk to reiterate their arguments, it is deemed nevertheless instructive to consider the following scenario. In a d^2-configured C_{4v} symmetrical ML_5 transition metal complex with a sq.-pyramidal coordination geometry, the initial small energy difference of the d_{xy} (b_2) and the degenerate d_{xz} and d_{yz} (e) orbitals is raisedon widening the metal centered angle φ between the apical and basal ligands from 90° (Figure 13).[39] Increase of the φ angle also significantly lowers the energy of the d_z2 orbital in that it is eventually lying below the degenerate set of the d_{xz} and d_{yz} orbitals (not presented in Figure 13). Considering the Cp ligand as a monodentate apical ligand L, this picture holds in principle also for $CpML_4$ complexes. As has been shown by R. Hoffmann et al. in their EHT analysis on the latter system,[40] the d_{xz} and d_{yz} orbitals are further raised in energy with respect to the dz^2 orbital due to additional $d\pi$-$p\pi$ interactions with the e_1' set (D_{5h} symmetry) of the cyclopentadienyl π-system. Therefore, just the rather low lying metal based d_{xy} and dz^2 orbitals will be occupied in $CpML_4$ systems; as will be shown below this is also observed for the complexes described herein.

In the absence of additional splitting of these levels due to π-acceptor ligands or, (to smaller extent) due to π-donors, it becomes readily apparent that these complexes display just small HOMO−LUMO gaps, Δ. In principle, the multiplicity of the ground state of the complex, i.e., singlet vs triplet state is determined by the relative sizes of Δ and the pairing energy, PE. If $\Delta < \mathrm{PE}$ a triplet state is preferred, which is likely to be the case for the system described above with an anticipated small Δ. Although this simplified picture is not rigorously correct, and readers are referred to R. Poli's excellent review for details,[10] it is quite self-instructive to explain the presence of *thermally populated* spin state equilibria in these systems with $\Delta \approx \mathrm{PE}$.

In an elegant study, Rothwell et al. established singlet−triplet spin state equilibria of this type for a pseudo-octahedral pyridyl phenoxy tungsten(IV) system with a formal 14-electron configuration.[9] These complexes display singlet ground states with the triplet state being partially thermally populated. The singlet−triplet energy gaps ΔE were determined quantitatively in toluene solution by fits of the observed temperature dependent ^{1}H NMR data to the Van-Vleck equation (eq 3).

The strong deviation from the Curie behavior of the temperature dependent ^{1}H NMR resonances (Figure 4) in the formal 16-electron configured cationic complexes **1-Me** and **1-NMe$_2$** and the similarity of the plots for the individual chemical shifts vs temperature (Figures 10 and 11) with the results of Rothwell et al. suggested also a singlet−triplet spin-state equilibrium for **1-Me** and **1-NMe$_2$** in CD_2Cl_2 solution. This contrasted the results observed for the related cationic molybdenum halfsandwich complexes with a pianostool geometry, i.e., $CpMoL_2X_2^+$, where L_2 is a mono- or bidentate phosphine donor and X is a halide ligand, which were found to have a *pure triplet* state in the temperature range of 4 K to 293 K.[17]

To establish that a Curie behavior could be observed for the cationic $Cp^*WCl_2(R_2\text{-bpy})^+$ system after all, we prepared and investigated the magnetic properties of the novel corresponding neutral d^3-W(III) complex, **2-Me**. The linear dependence of the ^{1}H NMR chemical shifts vs reciprocal temperature presented in Figure 4, clearly established a Curie behavior for **2-Me**. This supported the view that provided complexes **1-Me** and **1-NMe$_2$** inherited *pure triplet ground states*, one might observe a Curie dependence of their ^{1}H NMR shifts. Note, that this was eventually confirmed for complex **1-H** (Figure 5) in the course of our investigations.

To rule out other possible explanations for the observed ^{1}H NMR temperature dependence in complexes **1-Me** and **1-NMe$_2$**, we studied counterion (b) and concentration (equilibrium, (d)) effects for complex **1-Me.** The topic under item (b) was investigated through ^{1}H NMR measurements of **1-Me**^{BArF}, whereas (d) was studied by ^{1}H NMR spectroscopy at two different concentrations (10^{-1} and 10^{-3} M) of complex **1-Me**. In both cases, essentially unchanged ^{1}H NMR spectra were observed (Figure 6), which evidenced that deviations from the Curie behavior could be attributed to neither item (b) nor (d). This view was also supported through the perfect Lambert−Beer behavior observed for the bands in the UV/Vis spectrum of **1-Me**. In addition, we analyzed the ν(W−Cl) Raman spectroscopic data in complex **1-Me** both in the solid state and in solution to probe for possible isomers. Because just negligible differences of the ν(W−Cl) stretching frequencies (<5 cm^{-1}) were detectable in the solid state and solution spectra, there was no evidence for an additional species in solution. Although

(39) Albright, T. A.; Burdett, J. K.; Whangbo, M.-W. *Orbital Interactions in Chemistry*; John Wiley & Sons: New York, Chichester, Brisbane, Toronto, Singapore, 1985.
(40) Kubacek, P.; Hoffmann, R.; Havlas, Z. *Organometallics* **1982**, *1*, 180−188.

this did not unambiguously rule out the presence of other isomers with a different coordination geometry, e.g., a pseudo trigonal-bipyramidal structure, together with the results of the DFT calculations (vide infra) and previous studies by Hoffmann et al.,[40] we take this as a good hint that the square pyramidal structure observed in the solid state is also maintained in solution.

In sharp contrast to our previous findings and interpretation of the solution ^{1}H NMR data in dichloromethane, the magnetic susceptibility data of complex **1-Me** clearly evidenced a *pure triplet state* with zero-field splitting in the solid state (Figure 10). Because the bulk compound used in these measurements was essentially single crystalline material, it was deemed unlikely that its structure was different from the one observed by single-crystal X-ray diffraction. Further evidence for the distinct difference between the solution and solid-state magnetic susceptibility data was provided through magnetic susceptibility measurements in dichloromethane solution using the Evans method.[20,21] This is best illustrated by Figure 10, which includes both the solution and solid-state data for complex **1-Me**. The values of the temperature-dependent effective moment μ_{eff} vs T data in solution were not only significantly reduced, but also display a different temperature dependence. Obviously, these evidently contradicting results required a different rationale or, respectively, a refinement of the proposed singlet−triplet spin state equilibrium. Because we had no evidence for the presence of structural isomers in solution (vide supra) or further chemical equilibria, *solvation effects*, not present in the solid state, were accounted for the distinct difference. This was also hinted through the strong temperature dependence of the dielectric constant of the dichloromethane solvent used in these measurements, which almost doubles at −90 °C compared to its value at RT.[38]

To address this point, a solution study in a significantly less polar solvent than CH_2Cl_2 was sought. For these measurements, we resorted to $^{\mathbf{BAr^F}}$**1-Me**, which displays a significantly better solubility in low polar solvents owing to its partially fluorinated anion. This allowed to record vt ^{1}H NMR spectra in a 1:2 (v/v) mixture of CD_2Cl_2/toluene-d_8. As shown in Figure 7, despite some small curvature, an essentially linear dependence of the ^{1}H NMR shifts of $^{\mathbf{BAr^F}}$**1-Me** on the reciprocal temperature was observed. In contrast to *neat CD_2Cl_2* solvent, a *Curie behavior* with a *triplet ground state* could be therefore ascribed to $^{\mathbf{BAr^F}}$**1-Me** in this substantially *less polar* solvent mixture. Hence, this experiment provided strong support for the view that solvation strongly participated in the energetics of the two spin states. As will be shown below in the theoretical section, it is deemed that substantially better solvation of the $S = 0$ state is the prevailing mechanism.

In conclusion, items (a) − (d) pointed strongly toward a singlet−triplet spin state crossover with thermodynamically favorable singlet ground states for compounds **1-Me** and **1-NMe$_2$** in CD_2Cl_2 solution. For complex **1-H** on the other hand, a triplet ground state can be ascribed to this complex in both dichloromethane solution and the solid state.

For complexes **1-Me** and **1-NMe$_2$**, the quantitative determination of the singlet triplet energy gap in solution was therefore deemed possible and was attempted through fits of the vt ^{1}H NMR data to the Van-Vleck equation. As has been noticed in detail elsewhere,[14] such a fitting procedure is only valid, if the paramagnetic contributions to the chemical shifts originate exclusively from the *contact* (through bond) rather than from the pseudo-contact (dipolar, through space) shift term. Following a previously devised method,[14] the presence of a prevailing contact-shift term in the investigated compounds was confirmed by comparison of the bipyridyl proton resonances in the unsubstituted complex **1-H** and its methyl substituted congener, **1-Me**: Although the same signs of the paramagnetic shifts were observed for the proton resonances in the 3, 5, and 6 positions of the bipyridyl ring in complexes **1-H** and **1-Me**, the paramagnetic shifts of the bipyridyl methyl protons and the ring proton in the 4-position were found to display *opposite signs*. This clearly suggested that the prerequisite for the fit procedure described above was indeed fulfilled. It should be noted that it has been additionally conceived[9] that a successful fit of the NMR data to the Van-Vleck equation is also a reasonable indication for an exclusive/prevailing contact shift term. As shown below, this criterion was also fulfilled for complexes **1-Me** and **1-NMe$_2$**.

Initially, fits to the Van-Vleck equation in the form used by Rothwell et al. in the aforementioned successful study of tungsten(IV) complexes were attempted (eq 3).[9] It is noteworthy that fits to eq 3 were also used with success by other groups for other complexes, e.g., by Poli et al. for a Nb halfsandwich system.[41]

Using eq 3 the fits for complex **1-NMe$_2$** were apparently successful, which was evidenced through the small standard deviations for the derived values for ΔE and the diamagnetic shifts δ_{dia} for the individual protons, which were in the expected chemical shift range. However, for compound **1-Me** we encountered severe difficulties with the fit procedure. Although the fits converged and small standard deviations for the singlet triplet energy gaps were observed, we had to note that the derived δ_{dia} parameters converged not to their anticipated values. This is best explained for the chemical shift for the Cp* methyl protons, which converged at $\delta_{dia} = -20(\pm 2)$ ppm. Similar large deviations from their expected diamagnetic values ($\Delta\delta_{dia} = 7-9$ ppm) were also observed for the shifts of the residual aromatic and methyl protons of the bipyridyl ring. This clearly indicated an intrinsic problem with this fit procedure, respectively, with the description of the magnetic properties of these molecules. This was further substantiated by the aforementioned solid-state magnetic susceptibility data.

This prompted us to examine the Van-Vleck equation used in the form by Rothwell et al. in more detail (eq 3). The latter equation is clearly related to the more general form shown in eq 4. However, rather than using the entropy ΔS as a fourth fittable parameter, it is kept at a fixed value of $\Delta S = R \ln 3 = 9.1$ J mol^{-1} K^{-1} in eq 3. This value thus just equals the electronic term, ΔS_{el}, for the total entropic change of a singlet−triplet spin equilibrium with contributions from spin degeneracy. Additional terms of ΔS, e.g., vibronic contributions, ΔS_{vib}, and from solvation (vide infra) are thus ignored. For the free energy change $\Delta G_{S\to T}$ of the singlet−triplet spin equilibrium in solution, $\Delta G_{S\to T}$ can be written as

$$\Delta G_{S\to T} = \Delta G_{\text{gasphase},\, S\to T} + \Delta G_{\text{solv},\, S\to T} \qquad (5)$$

where $\Delta G_{gasphase}$ and ΔG_{solv} are the free energy changes in the

(41) Fettinger, J. C.; Keogh, D. W.; Kraatz, H.-B.; Poli, R. *Organometallics* **1996**, *15*, 5489.

gasphase and the free energy change of solvation of the singlet and triplet state. The latter can be estimated using the solvation model derived by Kirkwood et al., in which the solvent is described as a dielectric continuum with dielectric constant ϵ.[42] Including contributions from both monopoles (ions) and dipoles eq 6 is obtained. For a successful application and the discussion of the model the reader is referred to an excellent publication by T. J. Meyer et al., in which this model was used to describe the solvent dependence of metal-to-ligand-charge-transfer (MLCT) transitions[43]

$$\Delta G_{\mathrm{solv}}(T) = \frac{q^3}{2R}\cdot\left(\frac{1}{\epsilon} - 1\right) + \frac{\mu^2}{R^3}\cdot\left(\frac{1-\epsilon}{2\cdot\epsilon + 1}\right) \qquad (6)$$

The first term in eq 6 is the familiar Born model for the solvation of charged species,[44] which uses a point charge q at the center of the sphere with radius R, whereas the second equals the Onsager dipole solvation energy term for a compound with dipole moment μ.[45]

For the contribution of the solvation energy term to the energetics of the singlet−triplet spin equilibrium, the change of free enthalpy of solvation $\Delta G_{\mathrm{solv},S\rightarrow T} = \Delta G_{\mathrm{solv},T} - \Delta G_{\mathrm{solv},S}$ has to be considered. As will be shown below in the theoretical section, small geometrical changes are observed between the singlet and triplet states. This view is supported through the essentially identical volumes of the cationic complexes in **1-Me** ($S = 0$, $V = 465.0$ $S = 1$, $V = 466.7$ [Å^3] based on DFT calculations), which evidenced that the radii of the $S = 0$ and $S = 1$ ions are approximately equal, i.e., $R_{S=1} \approx R_{S=0}$. Because the charge q is unchanged in the singlet and triplet states, the first term of eq 6 therefore cancels out in the evaluation of $\Delta G_{\mathrm{solv},S\rightarrow T}$ leaving alone the dipolar term (eq 7)

$$\Delta G_{\mathrm{solv},S\rightarrow T}(T) = \frac{(\mu_T(\mu_T - \mu_S)\cos\phi)}{{R_{S,T}}^3}\cdot\left(\frac{1-\epsilon(T)}{2\cdot\epsilon(T)+1}\right) \qquad (7)$$

Because we want to focus on the temperature dependence of the free enthalpy of solvation with respect to the dielectric constant, the latter is denoted as temperature dependent, i.e., $\epsilon(T)$. The dependence of $\Delta G_{\mathrm{solv},S\rightarrow T}(T)$ on $\epsilon(T)$ seems to be rather complicated at first glance. Fortunately, the second term can be simplified for solvents displaying a somewhat higher polarity. As has been pointed previously,[43,46] this is based on the fact that the $(1 - \epsilon(T))/(2\epsilon(T) + 1)$ term becomes essentially linearly dependent on $1/\epsilon(T)$ for solvents with $\epsilon > 5$. For dichloromethane, which fulfills this criterion, eq 7 can be therefore written as (eq 8)

$$\Delta G_{\mathrm{solv},S\rightarrow T}(T) = \frac{(\mu_T(\mu_T - \mu_S)\cos\phi)}{{R_{S,T}}^3}\cdot\left(\frac{C}{\epsilon(T)} + C'\right) \qquad (8)$$

For a solvent with a negligible (small) temperature gradient of its dielectric constant, i.e., $\mathrm{d}\epsilon(\mathrm{T})/\mathrm{d}T \approx 0$, $\Delta G_{\mathrm{solv}}(T)$ is essentially temperature independent, i.e., $\Delta G_{\mathrm{solv},S\rightarrow T}\ (T) =$ constant. It should be noted that this criterion is essentially met for toluene, which has been used in the aforementioned measurements by the groups of Rothwell and Poli.[9,41] The situation is completely changed, however, if $\mathrm{d}\epsilon(\mathrm{T})/\mathrm{d}T$ for a solvent is large, which will lead to a significant temperature dependence of ΔG_{solv}. From the Debye law[47] it can be deduced that ϵ is proportional to $1/T$, i.e., $\epsilon(T) = C''T^{-1} + C'''$, where C'' and C''' are constants.[48] This is best illustrated with the data for dichloromethane using the $\epsilon(T)$ values determined by Morgan et al. already in the 1930s ($C'' = 3372.6$ K, $C''' = -2.48$).[38] Most importantly, the dielectric constant of dichloromethane displays a significant temperature gradient with a sharp increase upon lowering of the temperature; i.e., almost *doubling* of the dielectric constant is observed in going from 25 °C ($\epsilon = 8.9$) to − 90 °C ($\epsilon = 16.8$).[38]

Using $\epsilon(T) = C''T^{-1} + C'''$ eq 8 can be written as

$$\Delta G_{\mathrm{solv},S\rightarrow T}(T) = \frac{(\mu_T(\mu_T - \mu_S)\cos\phi)}{{R_{S,T}}^3}\cdot\left(\frac{C}{C''T^{-1} + C'''} + C'\right) \qquad (9a)$$

$$\Delta G_{\mathrm{solv},S\rightarrow T}(T) \approx \frac{(\mu_T(\mu_T - \mu_S)\cos\phi)}{{R_{S,T}}^3}\cdot(AT + B) \qquad (9b)$$

where A and B are constants.

Using the dielectric constants of dichloromethane at 8.9 and 16.8 at 298 and 193 K and with the assumption that the dipole moments and radii of the triplet and singlet state μ_{T} and μ_{S} and $R_{\mathrm{S,T}}$ are temperature independent, an increase of 7% is estimated for the absolute value of $|\mathrm{gD}G_{\mathrm{solv},S\rightarrow T}|$ upon lowering the temperature. Whether this interaction becomes more un/favorable depends on the relative size the dipole moments of the $S = 0$ and $S = 1$ solutes.

Furthermore, inspection of eq 9b immediately reveals that there is a temperature dependent and an independent term. Using the assumption that μ and R are temperature independent and grouping the terms to the *apparent* enthalpy and entropy of solvation $\Delta H_{\mathrm{solv,app}} = B/R^3\ \mu_T(\mu_T{-}\mu_S)\cdot\cos(\phi)$ and $\Delta S_{\mathrm{solv,app}} = -A/R^3\ \mu_T(\mu_T - \mu_S)\cdot\cos(\phi)$ leads to $\Delta G_{\mathrm{solv},S\rightarrow T} = \Delta H_{\mathrm{solv,app}} - T\cdot\Delta S_{\mathrm{solv,app}}$.

Using, $\Delta G_{\mathrm{gasphase}} = \Delta H_{\mathrm{gasphase}} - T\Delta S_{\mathrm{gasphase}}$, the free enthalpy of the spin transition process $\Delta G_{S\rightarrow T}$ in solution can be written as (eqs 10−11)

$$\Delta G_{S\rightarrow T} = (\Delta H_{\mathrm{gasphase}} - \Delta H_{\mathrm{solv,app}}) - T(\Delta S_{\mathrm{gasphase}} + \Delta S_{\mathrm{solv,app}}) \qquad (10)$$

$$\Delta G_{S\rightarrow T} = \Delta H_{\mathrm{apparent}} - T\Delta S_{\mathrm{apparent}} \qquad (11)$$

On the basis of eq 11 a four-parameter fit of eq 5 with $\delta_{\mathrm{dia},i}$, A_i, ΔH_{app} and ΔS_{app} as free variables was therefore deemed possible. It should be noted, however, that ΔH_{app} and ΔS_{app} cannot be interpreted in terms of a pure (gasphase or solid state) electronic singlet−triplet energy gap, because a contribution from solvation of unknown size is included. Nevertheless, the derived values allow to estimate equilibrium constants for the singlet−triplet spin equilibrium from the Van't-Hoff equation.

(42) Kirkwood, J. G. *J. Chem. Phys.* **1934**, *2*, 351.
(43) Kober, E. M.; Sullivan, B. P.; Meyer, T. J. *Inorg. Chem.* **1984**, *23*, 2098.
(44) Born, M. *Z. Phys.* **1920**, *1*, 45.
(45) Onsager, L. *J. Am. Chem. Soc.* **1936**, *58*, 1486.
(46) Reichardt, C. *Angew. Chem.* **1965**, *77*, 30.
(47) Atkins, P. W., de Paula, J. *Physical Chemistry*; 7th ed.; Oxford University Press: New York, 2002.
(48) Alternatively, a numerical expression of the $(1 - \epsilon(T))/(2\ \epsilon(T) - 1)$ term of dichloromethane can be obtained from a linear regression of the $(1 - \epsilon(T))/(2\ \epsilon(T) - 1)$ vs T data. For dichloromethane, this gave: $(1 - \epsilon(T))/(2\ \epsilon(T) - 1) = -0.511(1) + 3.06(6)\ 10^{-4}$ [K − 1] T with $R^2 = 0.997$.

The results from fits to eq 4 for complexes **1-NMe$_2$** and **1-Me** presented for all chemically inequivalent protons in Figures 8 and 9 clearly established the necessity to include an explicit entropic term as fourth fittable parameter. This can be immediately seen by inspection of the derived entropies ΔS_{app} for the spin-state equilibria (Table 4). The derived values for ΔS_{app} are in the order of 30 J mol^{-1} K^{-1} for both **1-Me (**29 eu**)** and **1-NMe$_2$** (37 eu) and are thus significantly larger than $\Delta S_{el} = R \ln 3 \approx 9.1$ J mol^{-1} K^{-1}. The most prominent difference between the magnetic properties of the two complexes manifested itself through the fitted values for ΔH_{app}. In accordance with the experimental and theoretical results, the dimethylamino substituted complex **1-NMe$_2$** displayed a substantially larger enthalpy for the spin equilibrium in comparison with the methyl substituted complex **1-Me**. The origin for this difference will be traced in the next section.

DFT Calculations. Further support for this view was sought from DFT calculations of the relative energies of the singlet and triplet states. However, an inherent problem of this procedure is that excited states are not correctly described by single Slater determinant methods. MCSCF/MRSCF DFT methods, on the other hand, which could appropriately deal with these systems are (currently) not affordable to deal with large systems.[49] It should be noted, however, that despite this inherent problem, DFT calculations were carried out in a number of cases to estimate the relative energies of different spin states. In the cases studied, they were found to produce rather reasonable results.[50−52] An additional inherent problem in the calculation of electronic/magnetic properties of 5d transition metals is the appropriate treatment of relativistic effects. Although scalar relativistic corrections were included through the usage of a relativistic Stuttgart−Dresden pseudopotential, spin−orbit (s−o) coupling was not accounted for in our calculations.[53] However, since the magnetic moments observed in our systems are close to the expected spin-only values it is deemed that the s−o contributions are negligibly small, thus validating our theoretical approach.

The calculations were carried out using the unrestricted formalism (UDFT) for the triplet and both restricted and unrestricted for the $S = 0$ states. With the aforementioned shortcomings of the applied DFT methodology kept in mind, the results of these calculations came nevertheless as a surprise. Although the calculated energy gaps between the singlet and triplet states in the gasphase were appreciably small and were hence in accordance with the experimental data, the ground states of complexes **1-R** were predicted to have *thermodynamically favorable* (12−21 kJ/mol) *triplet* rather than singlet states (Table 5). Prior to the measurements of the magnetic properties of **1-Me** in the solid state and further experimental data in solution, we accounted for this apparent contradiction between theory and experiment for **1-Me** and **1-NMe$_2$** by the inadequacy/unreliable accuracy of the DFT method.

In addition, we performed DFT calculations for the trigonal-bipyramidal isomers **1Me^{iso}**, **1-Me^{tbp}** (Figure 11). The latter were calculated to be 67 and 92 kJ/mol uphill from the square-pyramidal complex **1-Me** ($S = 0$). Because these values are far beyond the typical errors of DFT calculations, this clearly evidenced that these isomers do not play a role in the magnetochemistry of the tungsten(IV) system. In addition, we calculated the energy of the conformational isomer **1-Me^{rota}**, in which the Cp* ligand was rotated by 180° about the tungsten-centroid vector with respect to the geometry-optimized structure of **1-Me**. In accordance with our expectation, the total energy of **1-Me^{rota}** was found to be just 2 kJ/mol above **1-Me**.

Solvation Effects. Dichloromethane coordination to electrophilic cationic metal centers in transition metal complexes is well-established.[54] On the basis ofthe observation of a weak paramagnetism and weak W−Cl bonds in the corresponding neutral trichloride complex of **1-Me**, Cp*W(Me$_2$-bipy)Cl$_3$;[15] however, we did not expect that coordination of the CH_2Cl_2 chlorine lone pair could have lead to a stabilization of the singlet state in **1-Me**. Support for this was indeed provided through the failure to locate an energy minimum for such an η^1 or η^2 dichloromethane adduct, i.e., Cp*(Me$_2$-bpy)Cl$_2$W(ClCH$_2$Cl)$^+$ in the DFT calculation.

Therefore, we attributed the influence of the solvent to mere (undirected) solvation effects, i.e., a dielectric continuum. The influence of solvation on the relative energies of the spin $S = 0$ and $S = 1$ states in complexes **1-Me** was studied by DFT calculation using two different solvation models. We applied the COSMO dielectric continuum model of Klamt et al.[32] implemented in DMOL[33] as well as the self-consistent reaction field (SCFRM) method available in Jaguar.[36] In the latter model, the solvent was modeled at two different temperatures, i.e., at 180 and 298 K using the experimentally determined dielectric constants and densities. The derived relative energies of the two spin states for the geometry optimized CH_2Cl_2 solvated structures of complex **1-Me** compiled in Table 6 are in full accordance with the experimental findings. Although the triplet state is just slightly energetically favored over the $S = 0$ state in the SCFRM model, the DMOL/COSMO calculation predicts the singlet state to be the *ground state* of complex **1-Me** in CH_2Cl_2 at RT (Table 6).

MO Analysis. Previously, CpML$_4$ systems have been studied by several research groups at different levels of theory and were used to explain the observed preference for the pseudo sq.-py. coordination geometry and geometrical distortions found in a number of these complexes.[40,55,56] It deserves special mentioning that aside from the research of Poli et al.,[41,55] these investigations mostly centered on d^4 transition metal systems and bearing at least one ligand with a sizable π-acceptor propensity, i.e., carbonyl groups and, to a lesser extent phosphine donors. This contrasts the d^2-configured complexes **1** described herein, which incorporate excellent σ- and π-donor ligands. However, due to the absence of good acceptor groups in compounds **1**, the bipyridyl and cyclopentadienyl ligands have to "fill this gap" in the quite electron rich metal compounds − a fact which is clearly reflected in their structural and magnetic properties (vide infra).

At the outset of the discussion it should be noticed that the frontier orbitals of the $S = 0$ state, the HOMO and LUMO of

(49) Young, D. *Computational Chemistry: A Practical Guide for Applying Techniques to Real World Problems*; Wiley: New York, 2001.
(50) Smith, K. M.; Poli, R.; Legzdins, P. *Chem. Commun.* **1998**, 1903.
(51) Rodriguez, J. H.; Wheeler, D. E.; McCusker, J. K. *J. Am. Chem. Soc.* **1998**, *120*, 12 051.
(52) Legzdins, P.; McNeil, W. S.; Smith, K. M.; Poli, R. *Organometallics* **1998**, *17*, 615.
(53) Figgis, B. N.; Lewis, J. *Prog. Inorg. Chem.* **1964**, *6*, 37.
(54) For an example see: Arndtsen, B. A.; Bergman, R. G. *Science* **1995**, *270*, 1970.
(55) Poli, R. *Organometallics* **1990**, *9*, 1892.
(56) Lin, Z.; Hall, M. B. *Organometallics* **1993**, *12*, 19−23.

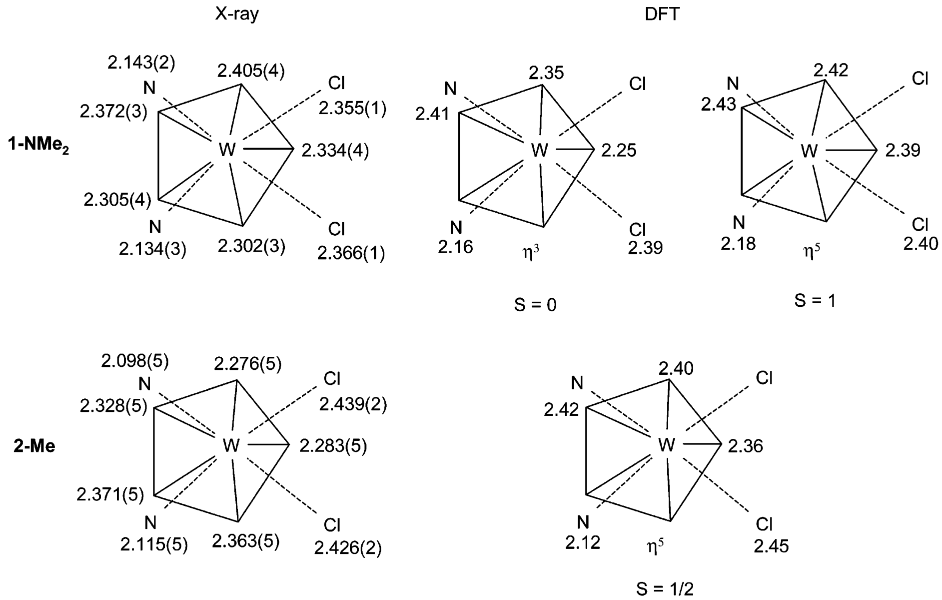

Figure 14. X-ray crystallographically determined and DFT calculated geometries ($S = 0$ and 1 states) of complex **1-NMe$_2$** (top trace) and complex **2-Me** (lower trace).

complexes **1** are also applicable for the triplet state (SHOMO and SSHOMO) and differ just by their electron occupation numbers. For comparison with the MO scheme of the C_{4v} symmetrical sq.-py. system presented in Figure 13, this analysis will be pursued with the coordinate system used there, i.e., the *z*-axis is pointing toward the Cp* ligand.

The inspection of the LUMO ($S = 0$) revealed contributions from both the metal center as well as the chloro and bipyridyl ligands (Figure 12). The metal character is constituted through the dz^2 orbital with some admixture of the d_{xy} orbital. In context with the further analysis presented below, we would like to draw the attention to the $d\pi-p\pi^*$ back-donation to the bipyridyl π^*-acceptor orbital, which partly compensates for the antibonding combination of the chlorine–tungsten $p\pi-d\pi$ donor interaction. It is noteworthy that in a previous analysis of d^2-configured Cp*ML$_4$ complexes by Poli et al., it was recognized that the strength of the π_C-$d\pi_{metal}$–acceptor interaction strongly influences the HOMO–LUMO gap, which in turn is dependent on the Cp$_{centroid}$–W–Cl angle.[41]

The metal character in the HOMO is easily recognized as the d_{xy} orbital (Figure 12). It displays an antibonding (π-donor) interaction between the chloro ligands and the tungsten center. In analogy to the LUMO, the latter is partly compensated by strong δ-bonding between the filled d_{xy} orbital and a Cp δ^*-acceptor orbital (e_2'' in local D_{5h} symmetry), which is schematically shown below.

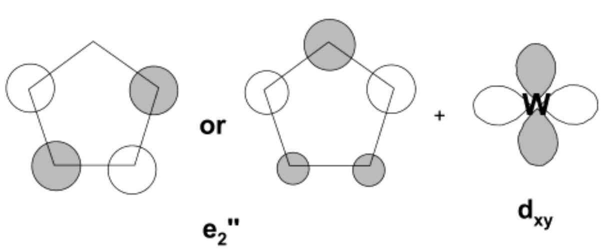

This type of interaction was first discussed by Hoffmann et al.[40] in the aforementioned EHT study on CpML$_4$ complexes and leads to a significant slippage of the metal center toward η^2/η^4, respectively, η^1/η^3-binding of the Cp ligand to maximize

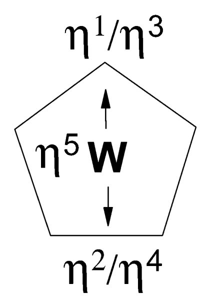

the overlap between the d_{xy} orbital and the Cp acceptor orbital ($e_2''^*$ in local D_{5h} symmetry). In the singlet state, this leads to a pronounced asymmetry for the binding of the Cp* ligand and is clearly reminiscent of an η^3-binding mode. This is best illustrated through the W–C distances observed in the optimized geometry of the $S = 0$ state of complexes **1**. This is also nicely reflected in the X-ray crystal structure of complex **1-NMe$_2$**, which according to the solid and in solution susceptibility measurements has a strong thermodynamic preference for the S = 0 state. This is further illustrated by the experimementally and DFT derived geometrical parameters for complex **2-Me**, which are also shown in Figure 14.

On the basis of the analysis of the frontier orbitals, a stronger stabilization of the LUMO is expected for bipyridyl ligands with a better π-accepting propensity, e.g., such as the unsubstituted ligand 2,2′-bipyridyl in complex **1-H**. Since the HOMO is *not* affected through substitution of the bipyridyl ligand, a smaller HOMO/LUMO gap and therefore a higher preference for the triplet state would be expected for this ligand metal combination. For weaker π-acceptors on the other hand, such as the dimethylamino bipyridyl ligand in complex **1-NMe$_2$**, a smaller stabilization of the LUMO (SHOMO for $S = 1$) thus leading to a thermodynamically more favorable singlet state would be anticipated. This rationale provides an excellent explanation for the experimentally observed reduced paramagnetism in **1-NMe$_2$** and, also, the triplet state found for complex **1-H** bearing the unsubstituted 2,2′-bipyridyl ligand.

In addition, it allows to explain the structural differences observed in X-ray crystal stuctures of complexes **1-Me** and **1-NMe₂**. In the $S = 0$ state, back-donation proceeds exclusively through δ−bonding, leading to a pronounced η^3-binding of the Cp* ligand in order to maximize overlap between the d_{xy} and the e_2''* Cp based orbital. In the triplet state, the latter interaction is significantly reduced due to additional dπ-pπ* back-donation, which consequently leads to more symmetrical (η^5) bonding of the Cp* ligand. This trend is very well reflected in the calculations (see Figure 14) and also experimentally through the X-ray crystal structure of complex **1-Me**.

Conclusion

The combination of experimental and theoretical methods, allowed to unambiguously unravel the magnetic properties of the novel cationic tungsten(IV) complexes both in solid state and in solution. The presented methodology is sought to provide strong guidelines for future studies in the field of solution and solid-state magnetochemistry.

Experimental Section

Reactions were carried out under a dinitrogen atmosphere using glovebox and Schlenk techniques. The halogenated solvents were thoroughly dried over P_4O_{10} and saturated with N_2. The other solvents were distilled under nitrogen from violet sodium benzophenone ketyl and stored under nitrogen. In addition, residual traces of water in the solvents and on the glassware, used in the synthesis and spectroscopic analysis of the highly water sensitive cationic complexes, were removed by either filtration over alumina (for CH_2Cl_2, Woelm, act. Super-I, neutral, previously dried at 10^{-5} Torr at 350 °C), or stirred over sodium−potassium alloy followed by filtration (ether, THF). The deuterated solvents were dried over sodium or P_4O_{10} and transferred in vacuo using high vacuum techniques. 2,2′-bipyridyl was purchased from Fluka and used as received. $Na(B(C_6H_3(CF_3)_2)_4)$ and $[Cp_2Fe]$-$[BPh_4]$ were prepared according to published syntheses.[57,58] The known dimer $[Cp^*WCl_2]_2$ was obtained from Cp^*WCl_4[59] using 1.5-fold excess of Zn dust in thf in analogy to the synthesis of $[(C_5H_4{}^iPr)WCl_2]_2$ reported by Green et al.[60] Complexes **1-Me** and **1-NMe₂** were prepared according to a route previously reported by us.[15] ^{1}H-, ^{19}F-, and ^{31}P NMR- spectra were recorded on Varian Gemini 200 and 300 spectrometers. Chemical shifts are given in ppm and referenced to the residual ^{1}H-solvent shift of a deuterated external sample or H_3PO_4 (85%, ^{31}P) or trifluorotoluene (^{19}F). Raman spectra were recorded on a Renishaw Ramascope spectrometer using HeNe (632.8 nm) excitation; UV/Vis-spectra were taken on a Cary 1E UV−Visible spectrometer. Mass spectra were measured with a Finnigan/MAT 8320 (MS) spectrometer and the peak assignments confirmed by a simulation of the isotope patterns. Molecular conductivities were determined in dichloromethane with an Amel-160 conductometer (glass cell, Pt, K = 1.0). Magnetic moments at RT were recorded with a Johnson−Matthey laboratory susceptibility balance and are corrected for diamagnetic contributions. Variable temperature solid state magnetic susceptibility measurements were performed with a Foner magnetometer at the University of Mainz by Dr. F. Tuczek. CHN-analyses were carried out with a LECO CHNS-932 elemental analyzer in our institute. The stoichiometric incorporation of solvent molecules into some of the analytically pure compounds was confirmed by either X-ray analysis or ^{1}H NMR integration.

(57) Brookhart, M.; Grant, A.; Volpe, F. J. *Organometallics.* **1992**, *11*, 3920.
(58) Brauer, G. *Handbuch der Präparativen Anorganischen Chemie*; Ferdinand Enke Verlag: Stuttgart, 1981; Vol. 3.
(59) Murray, R. C.; Blum, L.; Liu, A. H.; Schrock, R. R. *Organometallics* **1985**, *4*, 953.
(60) Green, M. L. H.; Hubert, J. D.; Mountford, P. *J. Chem. Soc., Dalton Trans.* **1990**, 3793.

X-ray Crystal Structure Analyses: General Remarks. Suitable single crystals were mounted on glass fibers in polyisobutylene oil (Aldrich, 38,896−6), transferred on the goniometerhead to the diffractometer and the crystal cooled to −90 °C in a N_2-cryostream. The data sets were collected with graphite monochromated Mo−Kα−radiation (0.70713 Å) on a Stoe IPDS image plate diffractometer. Intensities were corrected for Lorentz and polarization effects. Absorption corrections were performed numerically with the faces and crystal dimensions determined using the STOE Faceit-Video CCD camera system. The structures were solved using direct methods with the SHELXS-93 program package.[61] The refinements were carried out with SHELXL-97[62] using all unique F_o^2. All non-hydrogen atoms were treated anisotropically with the positions of the hydrogen atoms calculated in idealized positions (C−H bonds fixed at 0.96 Å) and refined as riding model. The details of the data collections and refinements including R-values are summarized in Table 1.

Synthesis of Cp*W(bpy)Cl₂, 2-H. 280 mg (0.359 mmol) $(Cp^*WCl_2)_2$ and 112 mg (0.718 mmol) bpy were dissolved in 20 mL THF in a high vacuum Young Teflon tap sealed Schlenk tube and degassed by three freeze pump thaw cycles. After heating in a vacuum for 2 d at 120 °C (behind a safety shield) a precipitate formed. Upon cooling to RT, the supernatant solvent was decanted off and the remaining solid washed 3× with toluene, followed by pentanes, and finally dried in high vacuum. The microcrystalline black, analytically pure product is insoluble in THF and slightly soluble in dichloromethane. Yield: 343 mg, (0.628 mmol), 88%. ^{1}H NMR (CD_2Cl_2, 298K), δ [ppm]: 24.5 (br, $\omega_{1/2} \approx 70$ Hz); 8.2 (br, $\omega_{1/2} \approx 130$ Hz); 4.5 (br, $\omega_{1/2} \approx 60$ Hz) −23 (vbr, $\omega_{1/2} \approx 500$ Hz); −34 (vbr, $\omega_{1/2} \approx 450$ Hz). MS (EI) *m/z* 546 (M$^+$). Magnetic moment (298 K): $\mu_{eff} = 1.67$ μ_B (corrected). Elemental analysis ($C_{20}H_{23}Cl_2N_2W$): Calcd. C, 43.98; H, 4.24; N, 5.13. Found. C, 43.75; H, 4.16; N, 5.13.

Synthesis of Cp*W(Me₂bpy)Cl₂, 2-Me. 315 mg (0.404 mmol) $(Cp^*WCl_2)_2$ and 149 mg (0.810 mmol) Me_2bpy were dissolved in 40 mL THF and transferred to a high vacuum Young Teflon tap sealed Schlenk. The mixture was degassed, heated for 4 d to 120 °C and then allowed to cool to RT. The supernatant solution was decanted off from the precipitate, which formed during the reaction. The solid was washed with toluene and pentanes and finally dried in high vacuum. The black microcrystalline material is moderately soluble in THF and dissolves well in dichloromethane. Yield: 390 mg, 0.680 mmol, 84%. ^{1}H NMR (CD_2Cl_2, 298 K), δ [ppm]: 84 (vbr, $\omega_{1/2} \approx 1300$ Hz), 22.6 (br, $\omega_{1/2} \approx$ 80 Hz); 3.8 (br, $\omega_{1/2} \approx 60$ Hz); 2.3 (br, $\omega_{1/2} \approx 80$ Hz) −45.5 (vbr, $\omega_{1/2}$ $\approx$ 800 Hz). MS (EI): *m/z* 574 (M$^+$). Magnetic moment (298 K): μ_{eff} $= 1.65$ μ_B. Elemental analysis ($C_{22}H_{27}Cl_2N_2W$): Calcd. C, 46.02; H, 4.74; N, 4.88. Found. C, 45.95; H, 4.82; N, 4.86. Single crystals suitable for X-ray diffraction were obtained by slow diffusion of ether into a solution of **2-Me** in 1,2-dichloroethane at RT.

Synthesis of [Cp*W(bpy)Cl₂][B(C₆H₃(CF₃)₂)₄], $^{BAr^F}$1-H. To a suspension of 216 mg (0.396 mmol) $Cp^*W(bpy)Cl_2$, **2-H**, in 20 mL dichloromethane, 201 mg (0.396 mmol) $[Cp_2Fe][BPh_4]$ was added in small portions under vigorous stirring upon which a color change from black to dark green and the formation of a green precipitate was observed. The volume of the solvent was concentrated to 5 mL in high vacuum and the supernatant solvent finally decanted off. The solid green residue was washed with toluene and pentanes and then dried in high vacuum giving 340 mg of the crude BPh_4^- salt, which was sparingly soluble in dichloromethane. The suspension of this material in 20 mL CH_2Cl_2 was reacted with 350 mg (0.396 mmol) $Na(B(C_6H_3(CF_3)_2)_4)$, stirred for 30 min at RT, then filtered through a sintered glassfrit. The product, $^{BAr^F}$**1-H**, was precipitated by slow addition of pentane to the filtrate, collected by filtration, washed with pentane and finally dried in high vacuum giving $^{BAr^F}$**1-H** as an analytically pure green solid.

(61) Sheldrick, G. M. *SHELXS-97; University of Göttingen: Göttingen, Germany 1997*.
(62) Sheldrick, G. M. *SHELXL-97, program for crystal structure solution nd refinement; Universität Göttingen, Germany 1993 and 1997.*

Overall yield: 66% (370 mg, 0.263 mmol). ^{1}H NMR (CD_2Cl_2, 298 K), δ [ppm]: 47.3 (br, $\omega_{1/2} \approx 60$ Hz); 37.8 (br, $\omega_{1/2} \approx 45$ Hz); 19.6 (br, $\omega_{1/2} \approx 40$ Hz); 7.72 (br, $[B(C_6H_3(CF_3)_2)_4]^-$); 7.56 (br, $B(C_6H_3(CF_3)_2)_4]^-$); -106.1 (br, $\omega_{1/2} \approx 180$ Hz); -109.5 (br, $\omega_{1/2} \approx 200$ Hz). ^{19}F NMR (CD_2Cl_2, 298 K), δ [ppm]: -63.8 (s, $[B(C_6H_3(CF_3)_2)_4]^-$). MS (FAB$^+$, CH_2Cl_2): *m/z* 545 (M^+). Magnetic moment (298 K): $\mu_{eff} = 2.41\ \mu_B$. Elemental analysis ($C_{52}H_{35}BCl_2F_{24}N_2W$): Calcd. C, 44.32; H, 2.50; N, 1.99. Found. C, 43.98; H, 2.55; N, 1.94.

Synthesis of $[Cp^*W(Me_2bpy)Cl_2][B(C_6H_3(CF_3)_2)_4]$, ^{BArF}1-Me. A solution of 90 mg (0.10 mmol) $NaB(C_6H_3(CF_3)_2)_4$ in 5 mL THF was slowly added to a suspension of 61 mg (0.10 mmol) $Cp^*W(Me_2bpy)Cl_3$ in 5 mL THF under stirring upon which a brown solution was obtained. The solvent was removed in high vacuum and the green solid residue dried for several hours in high vacuum. The product was extracted into 10 mL CH_2Cl_2 and filtered through a sintered glassfrit. Upon slow addition of pentane to the dark green solution a slightly oily precipitate was obtained, which was isolated by decanting the supernatant solvents off. The solid was dried in high vacuum to give 91 mg, (0.063 mmol) 63% **^{BArF}1-Me** as a dark green solid. ^{1}H NMR (CD_2Cl_2, 293 K, δ [ppm]): 113 (br s); 45 (br s); 30 (br s); 18.3 (br s); 7.72 (m, 8 H, $[B(C_6H_3(CF_3)_2)_4]^-$); 7.56 (m, 4 H, $[B(C_6H_3(CF_3)_2)_4]^-$); -92 (br s).

VT ^{1}H NMR Spectroscopy. The temperature calibration of the vt unit of the NMR spectrometer was performed using a calibration curve for the chemical shift differences of the methyl and OH protons of a standard methanol-H_4 sample. Temperature equilibration in the vt ^{1}H NMR experiments was allowed for at least 20 min. Measurements were performed in NMR tubes sealed with a Young Teflon tap with the samples being prepared in a glovebox under N_2 atmosphere. (<1 ppm O_2, H_2O) and finally degassed.

Fit of the VT ^{1}H NMR Data to the Van-Vleck Equation. The 4-parameter fits using eq 5 were performed with the Origin 5.0 (Microcal) program package using a Levenberg−Marquardt algorithm (Figures 10 and 11). Starting with different initial parameters for the hyperfine coupling constant A, δ_{dia}, ΔE (ΔH_{app} and ΔS_{app}), the fits converged also to the same values.

Determination of the Magnetic Moments: (a) Solid State. Room-temperature molar magnetic susceptibilities χ_m in the solid state were determined with a Johnson−Matthey laboratory magnetic balance in quartz tubes. The crystalline samples were crushed in an achat mortar, transferred to the tube and then sealed with a thick layer (3 mm) of Parafilm (preparations in glovebox). The given values are averaged values of several measurements, which showed only a small variance.[63]

(b) Solution. The magnetic susceptibility of complex **1-Me** was determined with the Evans-method in CD_2Cl_2 using a small amount of 1,2-dichloroethane as reference and a mixture of 1,2-dichloroethane and CD_2Cl_2 in a sealed capillary in the same NMR-tube as an external standard. The mass susceptibility was calculated from the chemical shift differences Δf of the 1,2-dichloroethane reference in solution and in the sample using the following equation[21]

$$\chi_g = \frac{3\Delta f}{4\pi fm} + \chi_0 + \frac{\chi_0(d_0 - d_S)}{m}$$

Corrections for temperature induced change of the solvent density were included using the data for CH_2Cl_2 given in reference.[38] Diamagnetic corrections of the molar susceptibilities χ_m were applied using either the independently determined susceptibilities of the free ligands or with the aid of the Pascal constants. The effective magnetic moments, μ_{eff}, were calculated from $\mu_{eff} = 2.828(\chi_m T)^{1/2}$.

DFT-Calculations. The applied methodology is described in the text. The restricted and unrestricted DFT calculations were performed with the Turbomole program suite and using the RI-DFT (BP-86 functional) and B3LYP implementation for the geometry optimizations and the calculation of the second derivatives. Essentially identical energy differences were obtained with the BP-86 functional using the *pure* DFT rather than the RI-DFT method. The parallel version of the Turbomole program package was used on our 24 CPU Linux cluster in all cases. For the DFT calculations including solvation the DMOL rel 3.5 (COSMO) and Jaguar rel. 4.1 (SCFRM) program packages were used.

Acknowledgment. We are indebted to Prof. Heinz Berke for his generous support. We would like to thank Professor Rinaldo Poli for pointing out the Van-Vleck fitting method for the determination of singlet triplet energy gaps. Comments and suggestions by Professor Ian Rothwell and Dr. Gerrit Luinstra on this work are appreciated. We would particularly like to thank Professor Felix Tuczek for the solid state magnetic susceptibility measurements and very stimulating discussions. Funding of this project by the Swiss National Science Foundation is gratefully acknowledged.

Supporting Information Available: Coordinates of DFT optimized structures and crystallographic information (PDF). This material is available free of charge via the Internet at http://pubs.acs.org.

JA028313C

(63) McMillan, J. A. *Electron Paramagnetism*; Reinhold Book Corporation: New York, 1968.